DYNAMIC BEHAVIOR OF A ROTATING COMPOSITE HOLLOW SHAFT

Bruno Ribeiro de Mendonça Gonçalves da Silva

Thiago Augusto Machado Guimarães

Aldemir Ap Cavalini Jr

Valder Steffen Jr

bruno@aero.ufu.br

thiago@mecanica.ufu.br

aacjunior@mecanica.ufu.br

vsteffen@mecanica.ufu.br

LMEst - Laboratory of Mechanics and Structures, Federal University of Uberlândia, School of Mechanical Engineering, Av. João Naves de Ávila, 2121, Uberlândia, MG, 38408-196, Brazil.

Abstract. *In this paper, a simplified homogenized beam theory (SHBT) is used in a preliminary numerical investigation regarding the dynamic behavior of a rotating composite hollow shaft. A horizontal flexible composite hollow shaft and a rigid disc compose the simple supported rotating system that is considered in the present contribution. The mathematical model of the rotor is derived from the Lagrange's equation and the Rayleigh-Ritz method, which is obtained by considering the strain and kinetic energies of the disc and hollow shaft, and the mass unbalance. Some simplifications are adopted in order to obtain the responses of the considered rotor system. Therefore, the proposed analysis is confined to the time and frequency domains. The orbits, unbalance responses, and Campbell diagram are determined for evaluating the dynamic responses. Further research efforts will be dedicated to additional numerical tests considering a finite element model and more sophisticated theories for the modeling of the rotating composite hollow shaft.*

Keywords: *Rotor system, composite hollow shaft, simplified rotor model, vibration responses, and Campbell diagram.*

1. INTRODUCTION

According to Ishida and Yamamoto (2012), research on rotordynamics has over 140 years of history. Its beginning was marked with the work of W.J. Macquorn Rankine (Rankine, 1869), in which the author mistakenly stated that it is impossible for rotating machines operating above a certain speed. This speed was later called critical speed for Dunkerley (1984). Simplified basics about rotating machines were approached by Jeffcott (1919). The work of H.H. Jeffcott led to the development of other essential researches, such as the Campbell diagram firstly presented by Wilfred Campbell from General Electric. More effective methods of balancing were proposed and the behavior of rotors supported by hydrodynamic bearings was further investigated, leading to the design of lighter rotating machines operating at higher speeds.

The mathematical representation of the specific physical phenomena that involve rotating machines requires a reliable design tool. In this context, the finite element (FE) method appears as a largely used technique for rotordynamics design. Nelson and MacVaugh (1976) were among the first researchers to include the effects of rotational inertia, gyroscopic moment, and axial force in the FE models. Before the FE method, the so-called transfer matrix method was used to determine the dynamic behavior of rotating machines considering the system as continuous one (Lallement, Lecoanet, Steffen Jr, 1982). In this context, the modern rotating systems currently employed in various industrial sectors were developed, such as steam turbines, hydro power units, and aircraft engines. These machines present high associated costs, operating with great responsibility and have already components made from composite materials.

Following the growing evolution of the materials used in rotating machines (i.e., materials associated with high performance and low weight), investigations on the dynamic behavior of composite shafts seems to be interesting. Besides applications in aircraft engines, Mazda adopts hybrid glass and carbon fiber shafts in their cars after 1982. The use of this new technology aims to reduce weight of the rotation system, the cost of maintenance, noise, vibration levels, and to increase efficiency when compared with the same components made with metals. Regarding aerospace applications, composite shafts are used in blades and helicopter rotors, and more recently in fixed wing aircraft, as shafts of actuation systems to operate control surfaces. These drive shafts are already used in aircrafts such as: Airbus A330, A340, A350, A380 and A400M, Bombardier C-Series, Boeing 787, and F-35 JSF (Crompton Technology Group Limited, website).

The rotating machine used in this paper is composed by a horizontal flexible composite hollow shaft and one rigid disc. The mathematical model of the rotor is derived from the Lagrange's equations and the Rayleigh-Ritz method. According to Lalanne and Ferraris (1998), the main phenomena that occur in rotordynamics can be evaluated by using this kind of model. Regarding the Lagrange's equations, kinetic energy expressions are used to characterize the disc, the hollow shaft, and mass unbalance. The flexible hollow shaft is described in terms of strain energy, using the Simplified Homogenized Beam Theory (SHBT) to find its stiffness (*EI*). The internal dumping of the hollow shaft is incorporated on the Lagrange's equations from its associated virtual work (Sino, Baranger, Chatelet, Jacquet, 2007).

2. COMPOSITE HOLLOW SHAFT

The hollow shaft studied in this contribution is a *roll wrapped carbon fiber tube* manufactured by *Easy Composites Ltd* (Easy Composites Ltd., website). The hollow shaft is manufactured from a special high-modulus Toray T700, unidirectional pre-impregnated carbon fiber ply oriented at 0° (i.e., along the length of the tube). *Crush/burst* strength is provided by a unidirectional *E-Glass* ply oriented at 90° (i.e., around the section of the tube). The analyzed material has five layers with the following stacking sequence: [0°, 90°, 0°, 90°, 0°]. Fig. 1 illustrates the analyzed composite shaft hollow. Tab. 1 summarizes the physic and geometric properties of the composite hollow shaft. Tab. 2 shows the mechanical properties of the analyzed composite material in comparison with the steel and aluminum materials.

Figure 1. Composite tube manufactured by *Easy Composites Ltd*

Table 1. Hollow shaft specification

Length (m)	Internal diameter (m)	Wall thickness (m)	Outer diameter (m)	Stiffness (EI, N·m^2)	Weight (kg)
1.0	0.014	0.00135	0.016	120	0.10

Table 2. Mechanical properties of the hollow composite shaft in comparison with other materials

Property	*Carbon Fiber Tube*	Steel	Aluminum
Density (kg/m^3)	1600	8000	2700
Youngs Modulus 0° (GPa)	90	207	72
Youngs Modulus 90° (GPa)	19	207	72
In-Plane Shear Modulus (GPa)	4.6	-	-
Major Poisson's Ratio	0.14	-	-

For sake of clarity, Fig. 2 presents a schematic representation of the fibers and rotor Cartesian directions. In this case, y is the longitudinal axis of the rotor (see Fig. 3), 1 is the fiber direction, 2 is the transversal direction related to the fibers in the ply, 3 is the perpendicular direction also related to the ply, and ϕ is the ply fiber angle.

4. ROTOR MODEL

Equation (1) presents the matrix differential equation able to models the dynamic behavior of flexible rotors (Lalanne, Ferraris, 1998):

$$[M]\{\ddot{q}\}+[C(\Omega)]\{\dot{q}\}+[K]\{q\}=\{F(t)\} \tag{1}$$

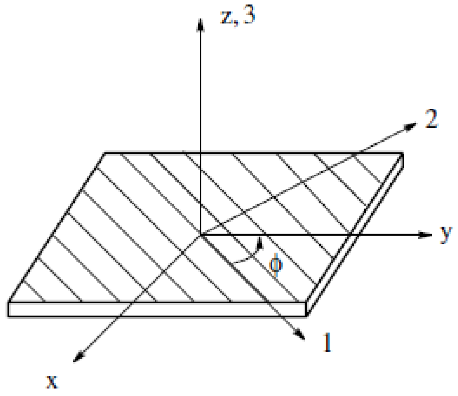

Figure 2. Plan of ply (Sino, Baranger, Chatelet, Jacquet, 2007)

where $[M]$ is the symmetric mass matrix, $[C(\Omega)]$ is the global asymmetric matrix including the antisymmetric gyroscopic matrix which depends on the rotational speed Ω, $[K]$ is the elastic stiffness matrix, $\{F(t)\}$ is the generalized force vector, and $\{\ddot{q}\}$, $\{\dot{q}\}$ and $\{q\}$ are respectively the acceleration, velocity, and displacement vectors.

Considering the dissipative effects associated with composite materials (Sino et al., 2006), Eq. (1) is them modified as shown by Eq. (2).

$$[M]\{\ddot{q}\}+[C_i+C(\Omega)]\{\dot{q}\}+[K+K_i(\Omega)]\{q\}=\{F(t)\} \tag{2}$$

where $[C_i]$ is the internal damping matrix and $[K_i(\Omega)]$ is the stiffness matrix which depends on the internal damping and also on the rotational speed Ω. According to Sino et al. (2007), the anisotropic properties of composite materials and their lightness can be used to optimize composite shafts in order to improve their dynamic behavior. Compared to metals, composite materials have higher damping capacities that can induce a destabilizing effect on the rotor motion.

As mentioned, the mathematical model of the rotor used in this work is derived from the Lagrange's equations and the Rayleigh-Ritz method. The rotor is assumed to be simply supported at both ends. Therefore, the displacements along the x and z directions, considering any y location along the shaft (see Fig. 3), are given by:

$$\begin{aligned} u(y,t) &= f_1(y)\, q_{11}(t) + f_2(y)\, q_{12}(t) \\ w(y,t) &= f_1(y)\, q_{21}(t) + f_2(y)\, q_{22}(t) \end{aligned} \tag{3}$$

The angular rotations θ_x and θ_z are small and they can be approximated as follows:

$$\begin{aligned} \theta_x(y,t) &= \frac{d f_1(y)}{dy} q_{21}(t) + \frac{d f_2(y)}{dy} q_{22}(t) \\ \theta_z(y,t) &= -\frac{d f_1(y)}{dy} q_{11}(t) - \frac{d f_2(y)}{dy} q_{12}(t) \end{aligned} \tag{4}$$

In this work, two displacement functions $f(y)$ are considered to determine the vibration responses of the rotor. The first and second vibration modes of a simple supported beam in bending are represented (beam with constant cross section). Thus, q_{11} and q_{21} from Eq. (3) are associated with the displacement function $f_1(y)$. The coordinates q_{12} and q_{22} are related with $f_2(y)$. The displacement functions can be seen in Eq. (5).

$$f_1\left(y\right)=\sin\frac{\pi y}{L}$$
$$f_2\left(y\right)=\sin\frac{2\pi y}{L} \tag{5}$$

As the rotor has constant geometric properties along its longitudinal y axis, the homogenized mechanical characteristics can be simplified, thus the potential energy and virtual work of the shaft can be expressed as given by Eq. (6).

$$U_s=\frac{1}{2}\int_0^L\left(EI_x\left(\frac{\partial\theta_x}{\partial y}\right)^2+EI_z\left(\frac{\partial\theta_z}{\partial y}\right)^2\right)dy$$
$$\delta W_s=\beta EI\int_0^L\left(\frac{\partial^2\dot{u}}{\partial y^2}\frac{\partial^2\delta u}{\partial y^2}+\frac{\partial^2\dot{w}}{\partial y^2}\frac{\partial^2\delta w}{\partial y^2}-\Omega\frac{\partial^2 w}{\partial y^2}\frac{\partial^2\delta u}{\partial y^2}+\Omega\frac{\partial^2 u}{\partial y^2}\frac{\partial^2\delta w}{\partial y^2}\right)dy \tag{6}$$

where β is a dimensionless parameter and the homogenized flexural inertias are:

$$EI_z=EI_x=EI$$
$$EI=\sum_{p=1}^{N}E_y^pI^p \tag{7}$$
$$I^p=\pi\frac{R_p^4-R_{p-1}^4}{4}$$

According to the SHBT theory, the Young's modulus of each ply can be obtained from Eq. (8).

$$E_y^p(\phi)=\frac{1}{\dfrac{c^4}{E_l}+\dfrac{s^4}{E_t}+c^2s^2\left(\dfrac{1}{G_{lt}}-2\dfrac{\upsilon_{tl}}{E_t}\right)} \tag{8}$$

where s and c are $\sin(\phi)$ and $\cos(\phi)$, respectively. E_l and E_t are the longitudinal and transversal Young's modulus of the fibers, G_{lt} is the shear modulus, and υ_{tl} is the Poisson's ratio.

The kinetic energy of the shaft can be expressed as follows:

$$T_s=\frac{1}{2}\int_0^L\left\{\rho S_s\left[\left(\frac{\partial u}{\partial t}\right)^2+\left(\frac{\partial w}{\partial t}\right)^2\right]+\rho I_s\left[\left(\frac{\partial\theta_z}{\partial t}\right)^2+\left(\frac{\partial\theta_x}{\partial t}\right)^2\right]+\Omega J_s\left[\theta_z\frac{\partial\theta_x}{\partial t}-\theta_x\frac{\partial\theta_z}{\partial t}\right]\right\}dy \tag{9}$$

where ρ is the density, S_s is the cross-section area, I_s is the transversal moment of inertia, and J_s is the polar moment of inertia.

The kinetic energy of the T_d and mass unbalance T_u are given by (Lalanne, Ferraris, 1998):

$$T_d=\frac{1}{2}\left[m_d f^2(l_1)+I_{dx}g^2(l_1)\right](\dot{q}_1^2+\dot{q}_2^2)-I_{dy}\Omega g^2(l_1)\dot{q}_1q_2$$
$$T_u=m_u\Omega d\left[\dot{u}\cos(\Omega t)-\dot{w}\sin(\Omega t)\right] \tag{10}$$

where m_d is the mass of the disc, l_1 is the position of the disk along the shaft $g(y) = \partial f(y)/ \partial y$, I_{dx} and I_{dy} are the disc moments of inertia around the x and y directions, respectively, m_u is the unbalance mass, and d is the distance between the mass to the center of the shaft.

Substituting Eq. (6), Eq. (9), and Eq. (10) into Lagrange's equations (Eq. (11)), the equations of motion of the composite rotor are obtained (Eq. (12)).

$$\frac{d}{dt}\left(\frac{\partial T}{\partial \dot{q}_i}\right) - \frac{\partial T}{\partial q_i} + \frac{\partial U}{\partial q_i} = Q_i \tag{11}$$

$$[M]_{4x4}\begin{Bmatrix}\ddot{q}_{11}\\ \ddot{q}_{21}\\ \ddot{q}_{12}\\ \ddot{q}_{22}\end{Bmatrix} + [C_i + \mathrm{C}(\Omega)]_{4x4}\begin{Bmatrix}\dot{q}_{11}\\ \dot{q}_{21}\\ \dot{q}_{12}\\ \dot{q}_{22}\end{Bmatrix} + [\mathrm{K} + K_i(\Omega)]_{4x4}\begin{Bmatrix}q_{11}\\ q_{21}\\ q_{12}\\ q_{22}\end{Bmatrix} = \{F(t)\}_{4x1} \tag{12}$$

The displacements along the x and z directions and the angular rotations θ_x and θ_z can be determined applying Eq. (3) and Eq. (4) on the responses obtained after the numerical integration of Eq. (12). The time responses of the rotating system were obtained by using the Newton-Raphson method in conjunction with the Newmark-type, trapezoidal rule integration algorithm.

5. NUMERICAL RESULTS

Figure 3 presents the rotating machine used in the numerical simulations studied in this work. It is composed of a horizontal composite hollow shaft (see Tab. 1) and one rigid disc positioned at y = 2L/3, where L is the length of the shaft. The physic and geometric characteristics of the disc are given by Tab. 3. The rotor is simply supported at points A and B (representation of the bearings). An unbalance of 1500 g.mm at 0° applied to the disc of the rotor was considered. Figure 4 shows the Campbell diagram of the considered rotor, in which the first critical speed in the analyzed frequency band is, approximately, 380 RPM (i.e., close backward and forward whirls). In this work, the dimensionless parameter β (Eq. (6)) was considered equal to $1x10^{-4}$.

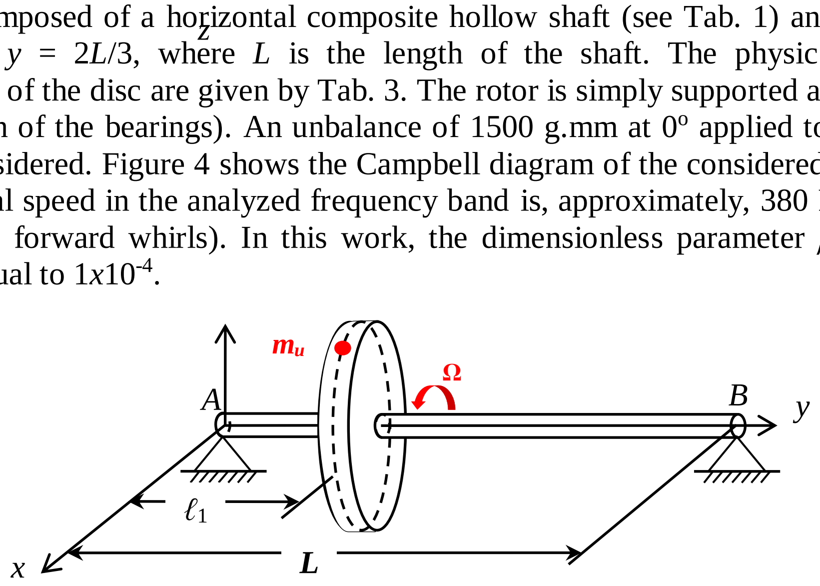

Figure 3. Schematic representation of the rotor

From the parameters given by Tab. 1 and Tab. 2, it was possible to obtain the stiffness (EI) of the hollow shaft by using Eq. (7) and Eq. (8). This result was compared with the one provided by the manufacturer, as shown in Tab. 4. Note that both calculated and manufacturer stiffnesses are close (difference of 0.6464%), which leads to the conclusion that the SHBT theory is able to represent the dynamic behavior of the hollow shaft used in this application (see Fig. 1).

Table 3. Disc parameters

Property	Value
Density (kg/m^3)	7800
Internal diameter (m)	0.016
Outer diameter (m)	0.2
Thickness (m)	0.02

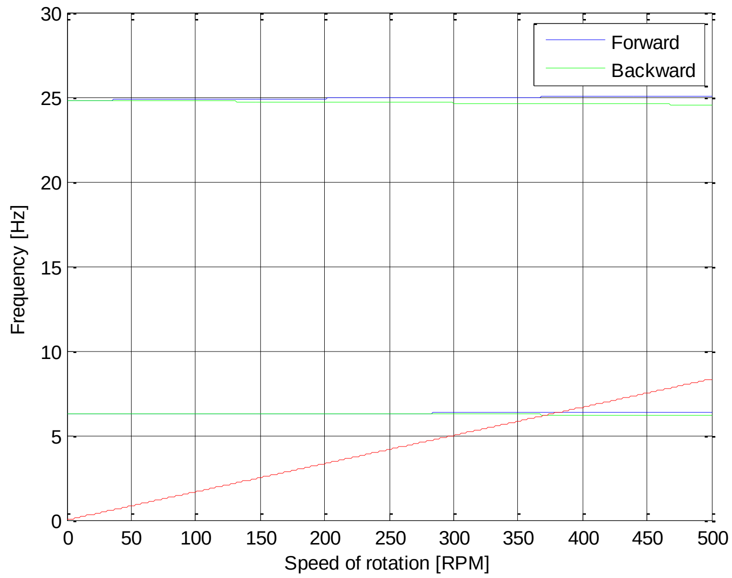

Figure 4. Campbell diagram of the analyzed rotor

Table 4. Tube stiffness using Simplified Homogenized Beam Theory

	Stiffness (EI, Nm^2)
Manufacturer data	120
SHBT theory	119.2293
Difference (%)	0.6464 %

Figure 5 shows the unbalance response of the rotor obtained along the *x* and *z* direction at the disc location. It can be observed that the rotor becomes unstable in the vicinity of its first critical speed. This result can be associated with the length of the shaft used in this application (i.e., 1 m), as well as the characteristics of the composite material considered. The instability threshold was determined by using the Routh-Hurwitz criterion, as presented by Lalanne and Ferraris (1998).

Figure 6 shows the vibration responses of the rotor measured along the *x* and *z* directions at the disc position considering the system under four different conditions, regarding the rotation speed of the system: 95 RPM (a quarter of the first critical speed), 190 RPM (half of the first critical speed), 285 RPM, and 500 RPM (above first critical speed). Note that the

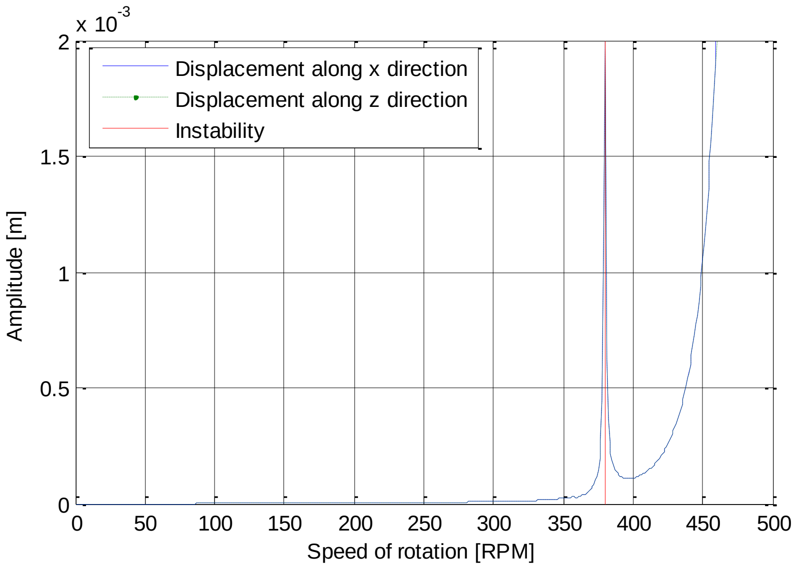

Figure 5. Unbalance response of the rotor and instability threshold

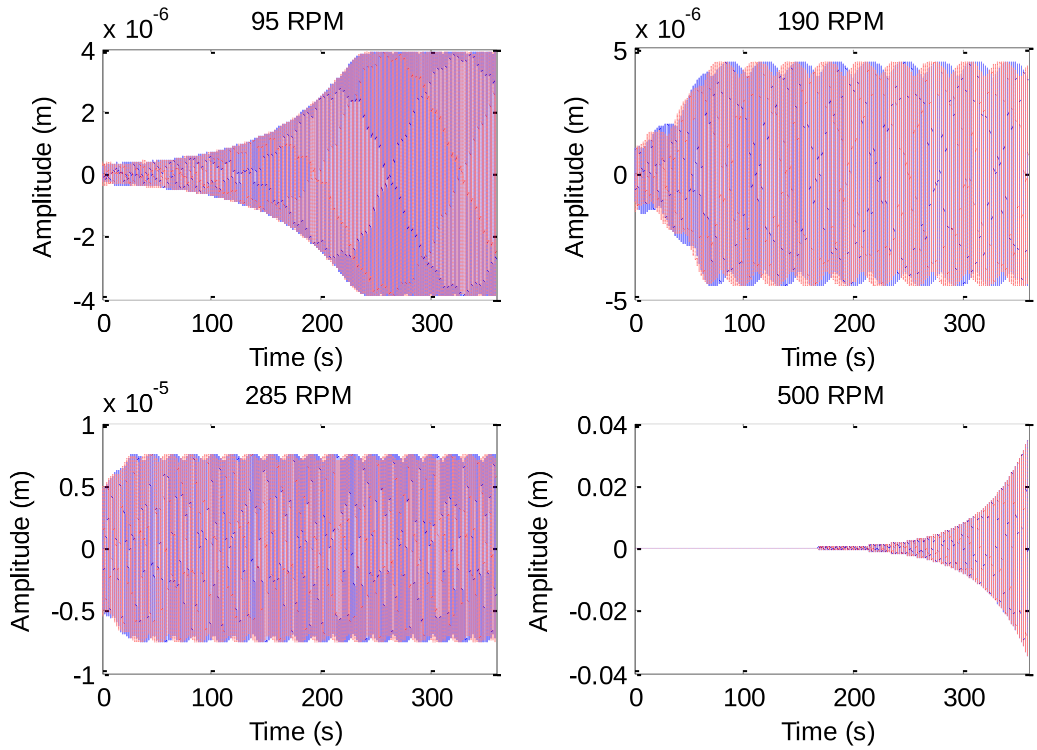

Figure 6. Unbalance response in the time domain for different speeds (---- *u*(*t*); ---- *w*(*t*))

rotor presents a stable operating condition for rotation speeds lower than the instability threshold (i.e., 95 RPM, 190 RPM, and 285 RPM). The unstable condition is demonstrated by the vibration responses obtained for the rotor operating at 500 RPM.

Details regarding the composite rotor vibrations are presented in Fig. 7. As expected, it can be observed that the dynamic behavior of the composite hollow shaft seems to be different of the ones obtained with the same components made with metals (i.e., a nonlinear behavior can be verified; see also the internal loops in Fig. 8).

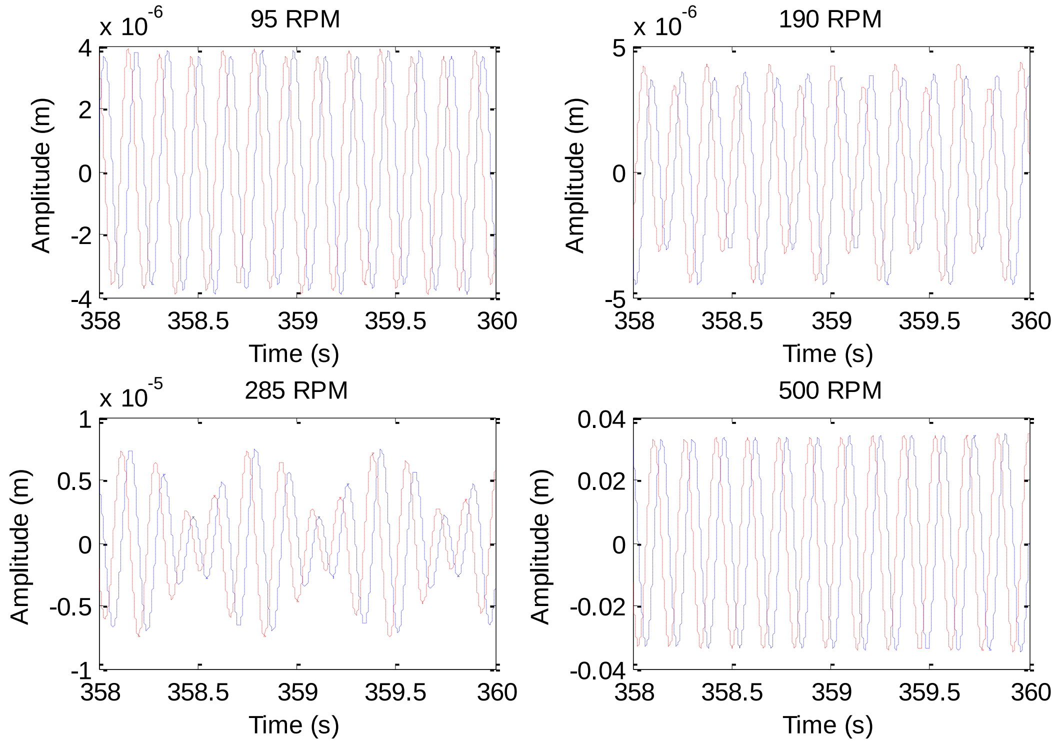

Figure 7. Unbalance response in the time domain for different speeds (---- *u*(*t*); ---- *w*(*t*))

Figure 8 shows the orbits obtained at the disc position considering the four rotation speeds analyzed in Fig. 6. Note that internal loops can be observed with the rotor operating under the mentioned conditions. In all scenarios, the scale of the horizontal and vertical axis are different in order to provided a better visualization of the orbits.

CONCLUSION

In this paper, a preliminary investigation regarding the dynamic behavior of a composite hollow shaft was discussed. The rotating machine used in the numerical analyzes is composed by a horizontal composite shaft and one rigid disc. The mathematical model of the rotor was derived from the Lagrange's equations and the Rayleigh-Ritz method. The proposed analyses were performed both in the time and frequency domains, as represented by the orbits, unbalance response, and the Campbell diagram. The orbits and unbalance responses were determined from different rotation speeds, in which the dynamic behavior of the considered hollow shaft could be analyzed. Further studies will encompass evaluations based on a finite element model for the rotor. An experimental verification is also scheduled.

ACKNOWLEDGEMENTS

The authors are thankful to the Brazilian Research Agency CNPq and to CAPES for the financial support provided to this research effort.

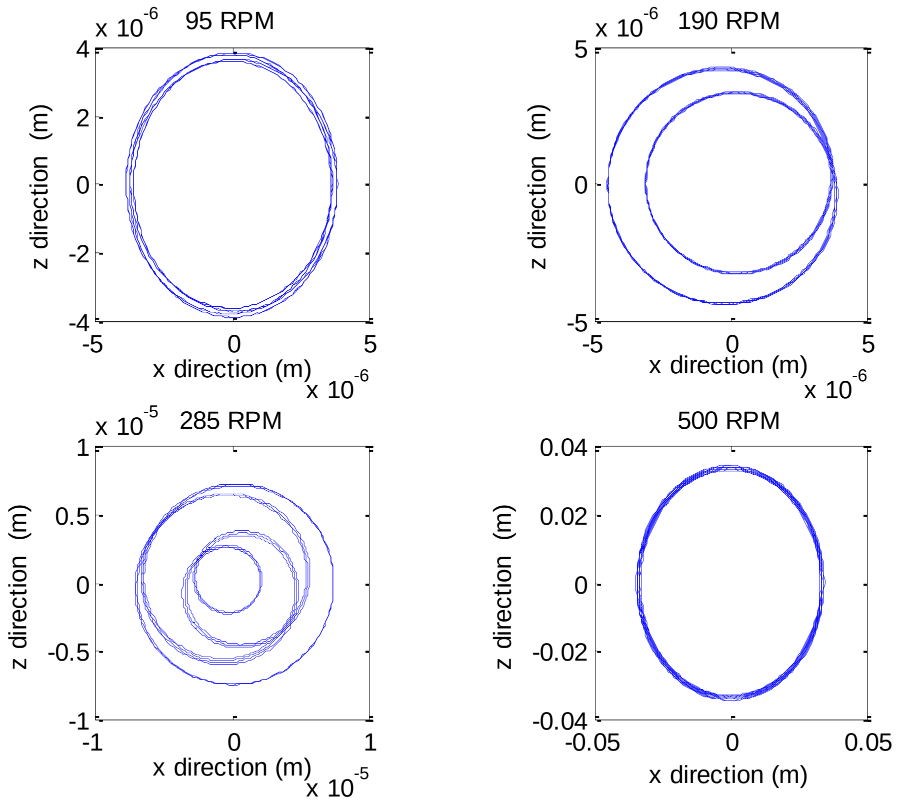

Figure 8. Orbits determined at the disc position for the rotor operating at different rotation speeds

REFERENCES

Crompton Technology Group Limited. *Transmission Shafts*. Website: <http://www.ctgltd.com/aerospace-composites >. Accessed on: April 18th 2015.

Dunkerley, S., 1984. On the whirling and vibration of shaft. *Philosophical Transactions of the Royal Society of London*, Vol. 195, n. 1, p. 279-359.

Easy Composites Ltd. *Carbon Fibre Tube*. Website: <http://www.easycomposites.co.uk>. Accessed on: April 18th 2015.

Ishida, Y., Yamamoto, T., 2012. *Linear and nonlinear rotordynamics*. Wiley-VCH.

Jeffcott, H.H., 1919. The lateral vibration of loaded shafts in the neighborhood of a whirling speed: the effect of want of balance. *Philosophical Magazine A*, Vol. 37, n. 1, p. 304-315.

Lalanne, M., Ferraris, G., 1998. *Rotordynamics prediction in engineering*. John Wiley & Sons, INC.

Lallement, G., Lecoanet, H., Steffen Jr, V., 1982. Vibrations de rotors sur paliers à matrice de raideur non symetrique. *Machine and Mechanism Theory*, Vol. 17, n. 1, p. 47-55.

Nelson, H.D., Macvaugh, J.M., 1976. The dynamics of rotor bearing systems using finite elements. *Journal of Engineering for Industry*, Vol. 98, n. 2, p. 593-600.

Rankine, B.J.M., 1869. On the centrifugal force of rotating shafts. *The Engineer*, Vol. 1, n. 1, p. 1.

Sino, R., Baranger, T.N., Chatelet, E., Jacquet, G., 2007. Dynamic Analysis of a Rotating Composite Shaft. *Composites Science and Technology*

Sino, R., Chatelet, E., Baranger T.N. and Jaquet-Richardet G., 2006. Stability analysis of internally damped rotating composite shafts considering transversal shear. *Proceedings of ISROMAC - 11*, Honolulu, Hawaii USA.